IKK remains active after the initial inductive stimulus.

The IKKα and IKKβ protein kinases, and not another component of the IKK complex, appear to be directly responsible for IκB phosphorylation. The minimal active IKK complex is apparently a dimer composed of IKKα or IKKβ (or both). These experiments also provide an explanation for the mechanism underlying the termination of the NF-κB activation response. Such inactivation is important because prolonged or chronic NF-κB activation can result in inflammatory disorders (*20*).

References and Notes

1. J. A. DiDonato, M. Hayakawa, D. M. Rothwarf, E. Zandi, M. Karin, *Nature* **388**, 548 (1997).
2. I. Alkalay *et al.*, *Mol. Cell. Biol.* **15**, 1294 (1995); J. A. Brockman *et al.*, *ibid.*, p. 2809; K. Brown, S. Gerstberger, L. Carlson, G. Franzoso, U. Siebenlist, *Science* **267**, 1485 (1995); Z. Chen *et al.*, *Genes Dev.* **9**, 1586 (1995); J. A. DiDonato, F. Mercurio, M. Karin, *Mol. Cell. Biol.* **15**, 1302 (1995); E. B. M. Traenckner *et al.*, *EMBO J.* **14**, 2876 (1995); S. T. Whiteside *et al.*, *Mol. Cell. Biol.* **15**, 5339 (1995); J. A. DiDonato *et al.*, *ibid.* **16**, 1295 (1996).
3. C. H. Regnier, H. Yeong Song, X. Gao, D. V. Goeddel, *Cell* **90**, 373 (1997).
4. E. Zandi, D. M. Rothwarf, M. Delhase, M. Hayakawa, M. Karin, *ibid.* **91**, 243 (1997).
5. F. Mercurio *et al.*, *Science* **278**, 860 (1997).
6. J. D. Woronicz, X. Gao, Z. Cao, M. Rothe, D. V. Goeddel, *ibid.*, p. 866.
7. I. Stancovski and D. Baltimore, *Cell* **91**, 299 (1997).
8. E. Zandi, D. Rothwarf, J. DiDonato, unpublished results.
9. Transfer vectors were constructed using the baculovirus transfer vector pAcSGHis NT-B (Pharmingen). All inserts were prepared by polymerase chain reaction (PCR). HA-tagged IKKα (the HA epitope is fused in frame to the second amino acid of IKKα) was generated by PCR using the primers 5′-TACTAGCTCGAGGATACCCTTACGATGTTCCTGATTACGCTGAGCGGCCCCCGGGG-3′ and 5′-AGCTATCGCGGCCGCTCATTGTGTTAACCAAC-3′. This fragment was digested with Xho I and Not I and cloned into the corresponding sites of pAcSGHis NT-B. In the resulting vector, the $(His)_6$ tag is upstream of and in frame with the HA epitope. A similar strategy was used to generate the transfer vectors for $(His)_6$-HA–IKKβ and $(His)_6$-FLAG–IKKβ. Primers for FLAG-tagged and HA-tagged IKKβ were 5′-AGCTATCGCGGCCGCGACTACAAGGACGACGATGACAAAAGCTGGTCACCTTCC-3′, 5′-AGCTAGCGCGGCCGCTACCCTTACGATGTTCCTGATTACGCTAGCTGGTCACCTTCC-3′, and 5′-TGACTCCCGGGTCATGAGGCCTGCTCC-3′. For the generation of recombinant viruses, we followed the manufacturer's (Pharmingen) recommendations for growth and maintenance of Sf9 cells, preparation of recombinant baculoviruses, and infection of the cells. For in vivo recombination, we transfected the transfer vectors and BaculoGold DNA into Sf9 cells using SuperFect (Qiagen). To prepare a control viral stock, we cotransfected Sf9 cells with unmodified pAcSGHis NT-B vector and BaculoGold DNA. After 5 days, culture supernatants were collected and amplified by two rounds of infection. For expression of both IKKα and IKKβ, the corresponding recombinant viruses were mixed in various ratios before infection of Sf9 cells. The efficiency of infection was determined by indirect double immunofluorescence using antibodies to HA and FLAG.
10. Recombinant $(His)_6$-HA–IKKα and $(His)_6$-FLAG–IKKβ proteins were produced in Sf9 cells after infection with high-titer recombinant viruses. The proteins were purified as described (*1*). Briefly, cell extracts were fractionated on Q-Sepharose and the fractions containing IKK were applied to an adenosine triphosphate (ATP) affinity column. Bound proteins were eluted with 20 mM ATP and applied to a Superose 6 gel filtration column. The fractions containing IKK (200 to 250 kD range) were then bound to Ni-Sepharose and washed extensively with AP buffer (500 mM NaCl, 1% Triton X-100, and 2 M urea) (*1*) and eluted with 200 mM imidazole. The eluted IKKs were either separated by SDS–polyacrylamide gel electrophoresis (PAGE) (8% gel) and visualized by silver staining or further purified by immunoaffinity chromatography with anti-FLAG (M2)–coupled Sepharose for IKKβ or anti-HA–coupled Sepharose for IKKα.
11. E. Zandi and Y. Chen, unpublished results. IKKα does not discriminate between full-length wild-type IκBα and the IκBα(A32/36) mutant as effectively as does IKKβ. In addition to Ser^{32} and Ser^{36}, IKKα and to a lesser extent IKKβ also phosphorylate sites close to the COOH-terminus of IκBα (*1*).
12. C. F. Barroga, J. K. Stevenson, E. M. Schwarz, I. M. Verma, *Proc. Natl. Acad. Sci. U.S.A.* **92**, 7637 (1995); J. A. McElhinny, S. A. Trushin, G. D. Bren, N. Chester, C. V. Paya, *Mol. Cell. Biol.* **16**, 899 (1996); E. M. Schwarz, D. VanAntwerp, I. M. Verma, *ibid.*, p. 3554.
13. Purified IKK proteins were cross-linked in the presence of bovine serum albumin (BSA, 1 mg/ml) in AP buffer containing 300 mM NaCl, 1% Triton X-100, and 2 mM ethylene glycol-*bis*(succinimidylsuccinate) (EGS; Pierce) for 20 min at room temperature. The cross-linker was inactivated by addition of 500 mM tris-HCl (pH 8.0). Cross-linked proteins were either immunoprecipitated (as described below) before separation by SDS-PAGE (4.5% gel) or directly subjected to SDS-PAGE. Proteins were visualized by immunoblotting with specific antibodies. For immunoprecipitation, the cross-linked IKK preparations were divided in two; one portion was immunoprecipitated with anti-IKKα and the other with anti-IKKβ. The immune complexes were separated by SDS-PAGE (4.5% gel) and proteins were transferred to a membrane and immunoblotted with an antibody to the other subunit than the one used for immunoprecipitation.
14. Various amounts of GST-IκBα (full-length) or GST-IκBα(1–54) were incubated with purified $(His)_6$-HA–IKKα or $(His)_6$-FLAG–IKKβ in kinase assay buffer (*1*) with 200 μM [γ-^{32}P]ATP for 20 min at 30°C. The reactions were stopped by adding SDS loading buffer, and proteins were resolved by SDS-PAGE (10% gel). The phosphorylated IκB bands were visualized and quantified by a phosphoimager (Bio-Rad). The amount of radioactivity in each band was plotted against the substrate concentration using a nonlinear regression program (SigmaPlot). The K_m values for each enzyme were determined from the corresponding plots.
15. For a review, see I. M. Verma *et al.*, *Genes Dev.* **9**, 2723 (1995).
16. S. C. Sun, P. A. Ganchi, D. W. Ballard, W. C. Greene, *Science* **259**, 1912 (1993).
17. F. Arenzana-Seisdedos *et al.*, *Mol. Cell. Biol.* **15**, 2689 (1995).
18. Full-length GST-IκBα or GST-IκBβ (2 μg) were incubated with an excess of purified NF-κB dimers formed from recombinant p50(NF-κB1) and the Rel homology domain of p65(RelA) [F. E. Chen, D. B. Huang, Y. Q. Chen, G. Ghosh, *Nature* **391**, 410 (1998)]. The GST-IκB-p50-p65 complexes were separated from free NF-κB by chromatography on glutathione–Sepharose 4B (Pharmacia). The ternary IκB–NF-κB complexes, whose formation was confirmed by SDS-PAGE and Coomassie blue staining, were washed with kinase buffer before kinase assay.
19. J. E. Thompson, R. J. Philips, H. Erdjument-Bromage, P. Tempst, S. Ghosh, *Cell* **80**, 573 (1995).
20. P. J. Barnes and M. Karin, *N. Engl. J. Med.* **336**, 1066 (1997).

21. We thank D. Rothwarf and F. Mercurio for insightful discussions and reagents; Z. Radic for help with kinetic analysis; G. Ghosh for purified NF-κB proteins (*18*); G. Cadwell for excellent technical assistance; and B. Thompson for help with manuscript preparation. E.Z. was supported by a junior postdoctoral fellowship from the American Cancer Society. Supported by NIH grant AI 43477 (M.K.).

19 May 1998; accepted 20 July 1998

Optimizing Gaze Control in Three Dimensions

Douglas Tweed,*† Thomas Haslwanter, Michael Fetter

Horizontal and vertical movements of the human eye bring new objects to the center of the visual field, but torsional movements rotate the visual world about its center. Ocular torsion stays near zero during head-fixed gaze shifts, and eye movements to visual targets are thought to be driven by purely horizontal and vertical commands. Here, analysis of eye-head gaze shifts revealed that gaze commands were three-dimensional, with a separate neural control system for torsion. Active torsion optimized gaze control as no two-dimensional system could have, stabilizing the retinal image as quickly as possible when it would otherwise have spun around the fixation point.

The human eye rotates with three degrees of freedom: horizontally, vertically, and torsionally (*1*, *2*). With few exceptions, theories of vision and eye movement have ignored rotations about the line of sight. One reason is Listing's law (*1*, *3*, *4*), which states that ocular torsion stays near zero during head-fixed gaze shifts. This has been taken as confirmation that gaze is driven by purely horizontal and vertical commands. Here we show that Listing's law is just one mode of gaze control, valid only when the head is stationary.

When eye and head join forces to transport the gaze line, the logistics are complex. For one thing, the eye is quicker than the head—it reorients more swiftly when an interesting object

D. Tweed, Departments of Physiology and Applied Mathematics, University of Western Ontario, London, Canada. T. Haslwanter and M. Fetter, Department of Neurology, University of Tübingen, Germany.

*Present address: Department of Physiology, Medical Sciences Building 3207, University of Toronto, 1 King's College Circle, Toronto, Ontario, M5S 1A8, Canada.

†To whom correspondence should be addressed.

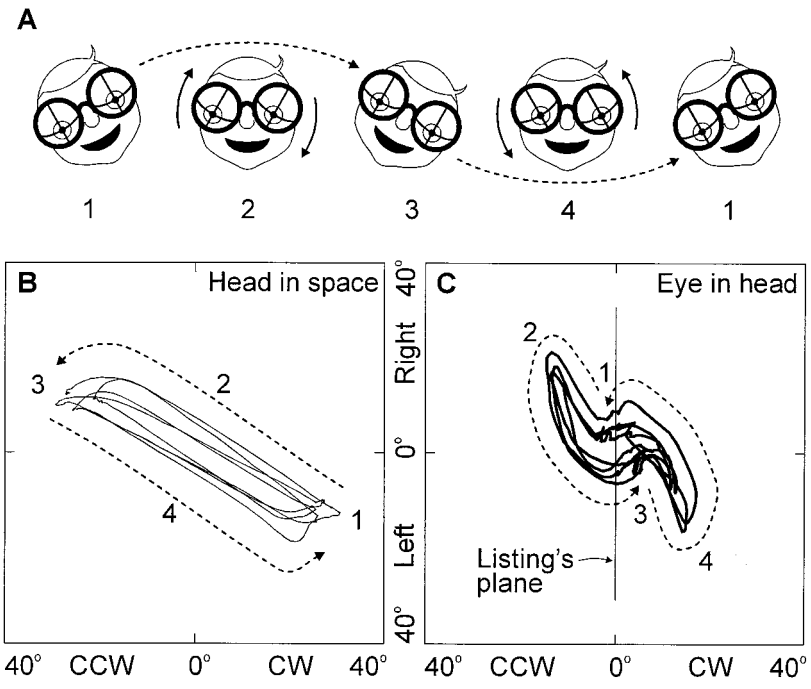

Fig. 1. (**A**) Gaze task. The person started in position 1, with the head turned ~30° CW and the eyes directed ~20° down in the head, looking at a laser spot projected on a spherical screen 1 m away. Then the spot jumped 20° to the right, and the person made an eye-head movement to refixate it. The head's contribution to this gaze shift, in keeping with instructions given beforehand (*7*), was a rolling movement ending up in position 3. After a brief pause, the laser spot jumped back to the person's left, evoking a movement back to position 1. Positions 2 and 4 show eye and head positions in mid-movement. (**B**) Angular head position in space during several repetitions of this task (*8*). Torsional head rotation (CW/CCW) is indicated on the abscissa; horizontal head rotation (right/left) is indicated on the ordinate. (**C**) The same components of eye position in the head. Vertical components are not shown in (B) and (C) because the motions were uneventful in that dimension.

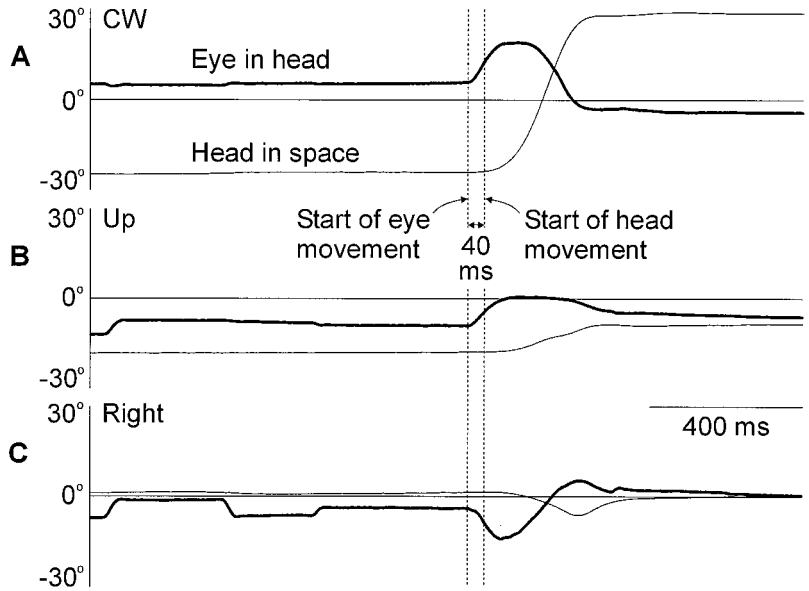

Fig. 2. Position versus time for the eye in the head (thick lines) and the head in space (thin lines). (**A**) Torsional eye and head motion. (**B**) Vertical motion. (**C**) Horizontal motion. The task is as in Fig. 1. For the first 1 s of the traces, the head is stationary and the eye makes small gaze shifts. Ocular torsion stays virtually constant at about 4° CW. Then the eye-head gaze shift begins: The head rolls almost 60° CW; the eye rapidly twists 15° CW and then reverses and rolls 20° CCW. This eye motion starts 40 ms before the head moves, which shows that it is not triggered by head-motion sensors in the inner ear.

appears in the visual periphery. The eye swivels rapidly to the visual target and locks on, whereas the head reorients itself more slowly (*5*, *6*). Computer simulations suggested that we could test for active control of ocular torsion by examining gaze shifts involving large torsional head rotations.

We chose a gaze task that was like watching a mouse darting back and forth along a floorboard (*7*) (Fig. 1A). In all study participants, the eye moved to its final position in space faster than the head, turning not just horizontally and vertically but also torsionally, so that midway through the movement, the eye was twisted far clockwise or counterclockwise (CW or CCW) relative to the head, as shown in panels 2 and 4 of Fig. 1A. It then held still in space as the head completed its motion. Panels B and C in Fig. 1 show a typical participant's head and eye rotations in this task (*8*). Each eye movement began and ended near the plane of zero torsion, called Listing's plane (*4*). It is known that static eye positions are slightly counterrolled when the head tilts (*2*), which is why the person's eye was twisted about 3° CCW in position 1 and about the same distance CW in position 3.

What was interesting was the eye's path. It did not simply jump between positions 1 and 3 but instead took exceptionally wide horizontal and torsional detours (*9*). For this person, the range of torsion amounted to 32°, from 17° CW to 15° CCW. Across all four participants, the torsional range varied between 22° and 34°, with an average of 29°. These ranges were enormous compared to the values of 2° to 4° that were seen during head-fixed gaze shifts (*4*).

Were these huge torsional excursions truly visually evoked gaze shifts, or were they driven by head-motion sensors in the vestibulum? They were not vestibular, because they were usually under way 20 to 60 ms before the head began moving (Fig. 2). Thus, the movements were not triggered by head motion but were voluntary gaze shifts (*10*).

The gaze task (Figs. 1 and 2) was chosen for its large torsional component, but everyday "looking around" also involves substantial head torsion, ranging over ±12° (*11*, *12*). When we tested one of our participants on natural eye-head gaze shifts to visual targets at 90° eccentricity (*7*), we found the same pattern: transient ocular torsion over ±6°, a range that was only 40% as large as that above, but still substantial. Thus the same motor strategy was used in both tasks, but the one in Figs. 1 and 2 better revealed the torsional potential of the system.

What was the purpose of the eye's transient torsion? As Fig. 1A suggests, the eye twisted to anticipate the coming torsional motion of the head. By so doing, it reached its final position in space long before the head motion was finished. From then on, the eye was stable in space, and so the visual world

remained stationary on the retina. Image blur was reduced (*13*), and visual analysis was simplified in other ways as well. For example, a stationary retinal image could be analyzed by a single set of orientation columns in the visual cortex, whereas a spinning image would excite a continuously changing array of columns (*14*).

So active torsion allowed the eye to stabilize its target image at the earliest possible moment. But this speed came at a price: As shown in Figs. 1C and 2, the eye took an indirect path relative to the head, spinning about the line of sight at up to 200° per second for 80 ms and then unwinding back to near-zero torsion over 200 ms. That the brain tolerated this detour showed that it put more weight on getting the eye on target quickly than on saving the eye muscles work.

To protect the orbital tissues, eye rotation is kept within certain boundaries (*6*)—about 40° horizontally and vertically and 15° torsionally. When these boundaries were taken into account, the eye trajectories in Fig. 1C could be explained quantitatively. Figure 3 shows a computer simulation of a model (*12*) that drove the eye as quickly as possible to its final position in space, given the above limits on its motion in the head. The resulting eye trajectories matched the data very well. The same model also mimics head-fixed gaze shifts and eye-head movements with more moderate head torsion (*12*), which suggests that all these movements are generated by a single gaze-control system.

The present data show that at least two aspects of this model are almost certainly correct. First, ocular torsion was under active neural control. The eye muscles were capable of rolling the eye over a torsional range of more than 30° (Fig. 1C), so the fact that torsion usually stays near zero (*1*, *3*, *4*) must reflect the careful tuning of the neural commands that activate the muscles. And this torsion-control system does not simply clamp ocular torsion, relative to the head, near zero. In our gaze task, it twisted the eye 15° CW or CCW, seeking a position in space that had been chosen so that, when the upcoming head motion was finished, the eye was back near Listing's plane.

Second, eye motion to a visual target was not determined by the retinal location of the target. We asked our participants to make the same gaze shifts as those shown in Fig. 1A, but with the head stationary. They held their heads still, 30° CW or CCW, as shown in panels 1 and 3, and they made head-fixed gaze shifts in response to the same visual input as before. Unsurprisingly, their eyes performed roughly fixed-axis rotations, staying within 2° of Listing's plane, as is usual in head-fixed gaze shifts (*4*). Gone were the wide loops with 15° of torsion. Thus the same sensory signals generated entirely different eye motions depending on whether a head movement was planned.

Our findings support the view that gaze is a three-dimensional control system, optimized to serve vision. When it wants to redirect the gaze line, the brain chooses desired orientations for the head and the eye, both defined in a space-fixed frame. Feedback loops drive head and eye toward their goals, though the eye's path may be deflected by its motion boundaries (*6*). The eye arrives at its target first and locks on, hanging suspended in space as the head rotates around it. When the head comes to a halt, ocular torsion relative to the head has returned to near zero, and the eye is poised for the swiftest possible response to the next visual target (*15*).

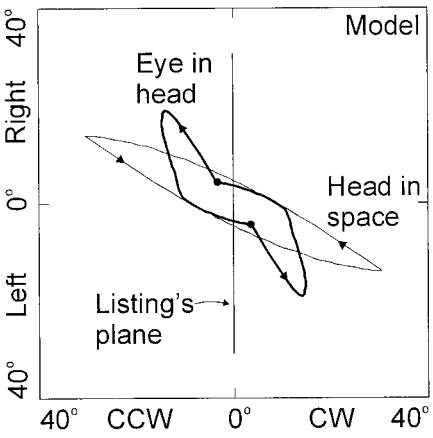

Fig. 3. A computer simulation of an optimized model of gaze control (*12*) matches the observed trajectories, including the eye's extreme deviations from Listing's plane. The eye stays near zero torsion between movements. During gaze shifts it takes the fastest possible path to its final position in space, with no constraint on torsion except that it stays less than 15° relative to the head.

References and Notes

1. H. von Helmholtz, *Handbuch der physiologischen Optik* (Voss, Hamburg and Leipzig, Germany, 1867).
2. P. A. Merton, *J. Physiol.* (*Proceedings*) **132**, 25 (1956); E. F. Miller, *Acta Oto-Laryngologica* **54**, 479 (1962).
3. L. Ferman, H. Collewijn, A. V. Van den Berg, *Vision Res.* **27**, 929 (1987).
4. D. Tweed and T. Vilis, *ibid.* **30**, 111 (1990); A. W. H. Minken, A. J. Van Opstal, J. A. M. Van Gisbergen, *Exp. Brain Res.* **93**, 521 (1993); D. Tweed, H. Misslisch, M. Fetter, *J. Neurophysiol.* **72**, 1425 (1994); D. Straumann, D. S. Zee, D. Solomon, A. G. Lasker, D. Roberts, *Vision Res.* **35**, 3321 (1995).
5. A. Roucoux, M. Crommelinck, J. M. Guerit, M. Meulders, in *Progress in Oculomotor Research*, A. F. Fuchs and W. Becker, Eds. (Elsevier, Amsterdam, 1980), pp. 309–315; V. P. Laurutis and D. A. Robinson, *J. Physiol. London* **373**, 209 (1986).
6. D. Guitton and M. Volle, *J. Neurophysiol.* **58**, 427 (1987); D. Tweed, B. Glenn, T. Vilis, *ibid.* **73**, 766 (1995).
7. Our four participants were healthy, aged 30 to 38, and gave informed consent. They were instructed to look to the target spot using a fast combined motion of eyes and head, with the head ending up 30° CW or 30° CCW. Similar results were obtained for torsional gaze shifts while looking up and for "natural" gaze shifts, in which the person was given no instructions about final head position but simply looked between four targets—up-right, down-right, down-left, and up-left—at 90° eccentricity. These latter gaze shifts were made in pseudorandom order and followed spoken commands.
8. The position of the left eye was recorded at 375 samples per second with the scleral-search-coil technique devised by D. A. Robinson [*IEEE Trans. Biomed. Electron.* **BME-10**, 137 (1963)]. Head position was recorded at the same rate with the use of search coils fastened to a lightweight bar molded to fit the person's teeth. Electrical signals from the eye and head search coils were converted to quaternions with the use of algorithms from D. Tweed, W. Cadera, and T. Vilis [*Vision Res.* **30**, 97 (1990)]. For an oculomotor introduction to quaternions, see G. Westheimer, *J. Opt. Soc. Am.* **47**, 967(1957); D. Tweed and T. Vilis, *J. Neurophysiol.* **58**, 832 (1987); or T. Haslwanter, *Vision Res.* **35**, 1727 (1995).
9. Our best performing participant showed a range of 16° CCW to 18° CW, tying the world record for human ocular torsion. A. P. Petrov and G. M. Zenkin [*Vision Res.* **13**, 2465 (1973)] also had a study participant who reached 18°, but by a different mechanism: Their participant was rotated torsionally in the dark; the eye movements were not gaze shifts to visual targets but vestibular responses to the head rotation, and they opposed the head's motion; whereas in our study the eye rolled the same way as the head and before it. R. Balliet and K. Nakayama [*Invest. Ophthalmol.* **17**, 303 (1978)] trained people to rotate their eyes torsionally while keeping their heads still. The training, which involved torsional visual feedback, allowed them to increase their torsional range by about 0.8°/hour, so that after 35 hours of training, the best performing person could move over a range of 26.5°. That result showed that the oculomotor system has torsional plasticity, whereas the present findings show that circuits for torsional gaze control are active in normal untrained humans. Our participants practiced the gaze task in Fig. 1 at most five times (that is, for only a few seconds) before recording began, and they showed the full torsional range of eye motion, or very close to it, on the first recorded trial.
10. The eye's return motion, when it came back toward Listing's plane while staying locked on the visual target, likely was vestibularly driven; but the initial outbound torsion, which anticipated the upcoming head turn, was not. In the outbound stage, the three-dimensional gaze system rotated the eye to its desired position in space and then locked on by activating the vestibuloocular reflex. This reflex uses vestibular information to monitor head velocity and counterrotate the eye, holding it steady in space as the head completes its motion (*5*, *6*).
11. P. Radau, D. Tweed, T. Vilis, *J. Neurophysiol.* **72**, 2840 (1994).
12. For model equations and predictions see D. Tweed, *ibid.* **77**, 654 (1997). In this model, eye and head are driven by two separate feedback loops to goal positions defined in space-fixed coordinates.
13. The loss of acuity caused by horizontal and vertical image slip depends on the spatial frequency of the image, which means that regions with a lot of fine detail are usually degraded more than coarse patches; see R. H. S. Carpenter, *The Movements of the Eyes* (Pion, London, 1988). Something analogous likely holds for the effects of torsional image slip on orientation detectors; radially oriented contours are degraded more than circumferential contours, so that the spokes of a spinning wheel are hard to make out, while the rim is clear.
14. J.-R. Duhamel, C. Colby, and M. Goldberg [*Science* **255**, 90 (1992)] reported that some visual cells in the parietal cortex adjust their receptive fields in anticipation of gaze shifts. Such cells will, for example, shift their receptive fields to the right immediately before rightward eye movements. Based on our results, one might also expect to find cells that adjust their receptive fields in the torsional dimension. For instance, an orientation-sensitive cell that normally responds best to horizontal lines may prefer CW-rotated lines in the final milliseconds before a CW gaze shift.
15. Advantages of rezeroing torsion are that the eye muscles probably require less force to hold an eye position near Listing's plane and that the eye, at the

center of its torsional range, is optimally placed for the next gaze shift, which may go either CW or CCW [see K. Hepp, *Vision Res.* **35**, 3237 (1995) and D. Tweed, *ibid.* **37**, 1939 (1997)].

16. We thank J. Dichgans, S. Ferber, V. Happe, C. Hawkins, M. Niemeier, and T. Vilis for comments on the manuscript. This work was supported by the Medical Research Council of Canada (grant MT-12847) and the Deutsche Forschungsgemeinschaft (grant SFB 307–A10).

31 March 1998; accepted 14 July 1998

Tree Species Diversity in Commercially Logged Bornean Rainforest

Charles H. Cannon,* David R. Peart, Mark Leighton

The effects of commercial logging on tree diversity in tropical rainforest are largely unknown. In this study, selectively logged tropical rainforest in Indonesian Borneo is shown to contain high tree species richness, despite severe structural damage. Plots logged 8 years before sampling contained fewer species of trees greater than 20 centimeters in diameter than did similar-sized unlogged plots. However, in samples of the same numbers of trees (requiring a 50 percent larger area), logged forest contained as many tree species as unlogged forest. These findings warrant reassessment of the conservation potential of large tracts of commercially logged tropical rainforest.

Conservationists have despaired over destruction of tropical rainforest by logging, clearing, and burning. Most extant tropical rainforest has been logged or will be in the near future, with only relatively small fragments preserved (*1, 2*). Thus, commercially logged forest with low residual timber value is the only remaining option if large areas of tropical rainforest are to be conserved. The diversity of trees is fundamental to total rainforest biodiversity, because trees provide resources and habitat structure for almost all other rainforest species. In specially controlled, low-impact logging trials in Queensland, Australia, tree diversity was maintained (*3*). However, more typical of commercial, selective logging is the use of heavy machinery to remove marketable species; this kills additional trees, damages soils, alters habitat, and reduces timber growth potential (*4, 5*). Reductions in tree diversity might be anticipated, but the effects of commercial logging on tree species diversity over vast areas of rainforest in Southeast Asia, Latin America, and Africa remain largely unknown (*1, 6*).

Comparisons between logged and unlogged forest can be confounded by differences in soil, topography, and disturbance history that influence whether a site will be logged. We chose a site that allowed for controlled comparisons, including areas logged at different times in the past (1 year and 8 years before sampling) and which had already been surveyed for the gross, structural effects of logging (*4*). Loggers were unaware that the effects of logging would be assessed. At low elevations in West Kalimantan, Indonesia, local-scale topographic variation restricts mechanized logging; commercially valuable, well-drained lowland dipterocarp forest is frequently intermixed with patches of swamp forest impassable to heavy machinery. In the logging concession we studied, lowland dipterocarp forest (59% of area) and swamp forest (41%) form a complex spatial mosaic (*4*). Machine operators cannot reach all areas of lowland forest without long search paths and prohibitive costs. Patches (0.5 to 10 ha) that escape logging are determined by the placement of logging roads and the haphazard search patterns of operators, rather than by intrinsic differences among patches (*4*); thus, these patches provided convenient unbiased unlogged controls.

The unlogged lowland forest is species-rich, but the commercial species (mainly *Shorea laevis*, *S. hopeifolia*, and *Dryobalanops beccarii*, in the family Dipterocarpaceae) dominate, comprising 70% of total precut basal area (*7*). Logging removed 62% of dipterocarp basal area and 43% overall. One year after logging, 45% of lowland forest canopy was open or dominated by low pioneer vegetation (including roads and skid trails), 15% was unaffected, and 40% was disturbed in varying degrees (*4*).

Logging reduced both tree density and the number of tree species per 0.1-ha plot, for both large and small trees (unlogged versus 1-year sites; Table 1). For all trees >20 cm in diameter (*7*), density fell by 41% and the number of species per plot by 31%. The species-area curves 1 year after logging fell well below those for unlogged forest (Fig. 1, A and B). However, per plot richness alone is inadequate for assessing logging effects on tree diversity. In highly diverse communities, where rare species have few or single individuals in plot samples, the number of species per plot is sensitive to reductions in density by random deletions of individuals—"rarefaction" (*8*). If mortality due to logging were equivalent to rarefaction alone, the underlying species-individual relationship would be unchanged. Then it would only be necessary to sample proportionately larger areas in logged forest to obtain similar numbers of individuals, and thus similar species richness, to unlogged

Table 1. Numbers of species and abundances of trees, comparing plots logged 1 year and 8 years before sampling and plots unlogged at the time of sampling. Small trees are 20 to 30 cm in diameter (at 1.37 m high); large trees are >30 cm in diameter. U-1, 1-8, and U-8 are *P* values for Scheffe pairwise tests comparing unlogged versus 1-year logged forest, 1-year versus 8-year logged forest, and unlogged versus 8-year logged forest, respectively. Asterisks denote significance at $\alpha = 0.05$. See (*15*) for sampling details. ANOVA, analysis of variance.

	ANOVA		Plot means			Scheffe pairwise tests		
	F	*P* value	Unlogged	1 yr	8 yr	U-1	1-8	U-8
			Trees per plot					
All trees	11.43	0.0002*	23.8	14.1	15.8	0.0004*	0.77	0.0007*
Large trees	7.51	0.002*	12.5	7.2	7.8	0.005*	0.93	0.02*
Small trees	4.41	0.02*	11.3	6.9	8.0	0.03*	0.80	0.15
			Species per plot					
All trees	5.04	0.013*	18	12.4	13.7	0.02*	0.81	0.11
Large trees	4.29	0.023*	9.7	6.6	6.6	0.05*	0.99	0.07
Small trees	6.12	0.006*	10	5.7	7.8	0.006*	0.30	0.27
			Species per individual					
All trees	4.6	0.02*	0.75	0.85	0.89	0.14	0.59	0.02*
Large trees	2.9	0.07	0.80	0.92	0.89	0.09	0.90	0.26
Small trees	3.9	0.03*	0.90	0.83	0.98	0.34	0.03*	0.37

C. H. Cannon, Department of Botany, Duke University, Durham, NC 27708, USA, and Institute of Biodiversity and Environmental Conservation, University of Malaysia, Sarawak, Malaysia. D. R. Peart, Department of Biological Sciences, Dartmouth College, Hanover, NH 03755, USA. M. Leighton, Department of Anthropology, Harvard University, Cambridge, MA 02138, USA.

*To whom correspondence should be addressed. E-mail: chc2@duke.edu